

Supplementary Information

The Collective Behavior of Spring-like Motifs Tethered to a DNA Origami Nanostructure

Elisa-C. Schöneweiß and Barbara Saccà*

Content

1. Materials and methods
2. Calculation of the effective spring constant of a set of springs
3. Application of the worm-like chain model
4. Design of the tethered hairpin motifs
5. Temperature-dependent FRET spectroscopy
6. Temperature-dependent UV spectroscopy

1. Materials and methods

All unmodified oligonucleotides were purchased from Sigma-Aldrich as desalted products and delivered lyophilized in 96-well plates. 6-carboxyfluorescein (FAM), carboxytetramethylrhodamine (TAMRA) and biotin-modified oligonucleotides were purchased from Sigma Aldrich in HPLC purification grade and used without further treatment. Single-stranded M13mp18 DNA, propagated in E.coli XL1-Blue (Agilent technologies; cat. # 200249) was produced from phage DNA (Affymetrix; cat. # 71706) as previously reported.¹ Ultrafree-DA Amicon centrifugal filter devices (100,000 Da MWCO, cat. # UFC5003BK) were purchased from Millipore. Water was purified on a Milli-Q® Integral Water Purification System (cat. # Z00QSVC01) and further filtered on 0.22 µm membrane filters (cellulose acetate, sterile, cat. # 28145-477) supplied by VWR. 1 kbp DNA ladder was purchased from Roth and agarose from Biozym (cat. # 84004). Agarose was purchased from Biozym (cat. # 84004), ethidium bromide staining solution from Merck (cat. # 1116080030). Buffers used were 1X TEMg (20 mM Tris base, 2 mM EDTA, 12.5 mM MgCl₂, pH 7.6), 1X TBEMg (40 mM Tris base, 20 mM boric acid, 2 mM EDTA, 12.5 mM Mg acetate, pH 8.0) and 1X TAEMg (40mM Tris base 20 mM acetic acid, 2 mM EDTA, 12.5 mM magnesium acetate, pH 8).

2. Calculation of the effective spring constant of a set of springs

2.1. Set of springs in parallel

In our origami structure, the hairpin motifs are identical, tethered to the central seam and aligned in parallel. We idealized the unfolding process of a single hairpin motif to the extension of a spring, with elastic constant k . Thus, considering two springs in parallel (as represented in Fig. S2), the displacement Δx will be the same for both and thus the resulting total force (F_{par}) can be calculated from the spring constant of the first (k_1) and second (k_2) spring as follows:

$$\begin{aligned}\Delta x_1 &= \Delta x_2 = \Delta x \\ F_{par} &= (k_1 \times \Delta x_1) + (k_2 \times \Delta x_2) = (k_1 + k_2) \times \Delta x \\ k_{par} &= k_1 + k_2\end{aligned}\tag{Eq. 1}$$

In general, the global action of n springs in parallel may be regarded as equivalent to the action exerted by a single spring with an additive spring constant.

$$F_{par} = \sum_{i=1}^n F_i = \sum_{i=1}^n (k_i \times \Delta x) = \left(\sum_{i=1}^n k_i\right) \times \Delta x = k_{par} \times \Delta x\tag{Eq. 2}$$

$$k_{par} = \sum_{i=1}^n k_i\tag{Eq. 3}$$

which, for identical spring-like elements, as in our construct I, simplifies to the following equation

$$\begin{aligned}k_1 &= k_2 = \dots = k_i = k \\ k_{par} &= nk\end{aligned}\tag{Eq. 4}$$

2.2. Set of springs in series

Consider two springs in series, which can have distinct spring constants, say k_1 and k_2 (Fig. S3). We now apply a common force F , which will result into two distinct displacements, namely Δx_1 for the first spring and Δx_2 for the second spring. As the force is the same for both springs, the following expression is valid:

$$\begin{aligned}\Delta x_{tot} &= \Delta x_1 + \Delta x_2 \\ F_{ser} &= k_1 \times \Delta x_1 = k_2 \times \Delta x_2 = k_{ser} \times \Delta x_{tot}\end{aligned}\tag{Eq. 5}$$

from which one can calculate how the effective spring constant is related to the spring constants of the single elements (in series):

$$\frac{1}{k_{ser}} = \frac{1}{k_1} + \frac{1}{k_2}\tag{Eq. 6}$$

If we now consider to have n pairs of springs in parallel, the total spring constant will be related to the spring constants of the two elements by the following relation:

$$\frac{1}{k_{tot}} = \frac{1}{n} \left(\frac{1}{k_1} + \frac{1}{k_2} \right)\tag{Eq. 7}$$

In case the two springs are identical, with spring constant k , the expression above becomes:

$$k_{tot} = \frac{n}{2} k\tag{Eq. 8}$$

This means that a system with two identical and parallel sets of hairpin motifs, connected one another in series, is equivalent to a system with one single set of hairpins in parallel having half spring constant (Fig. S4).

3. Application of the Worm-Like Chain (WLC) model

We treated the tethered DNA hairpin motif as a semi-rigid chain and applied the WLC approximation to calculate the entropic forces acting at the 5'- and 3'- extremities of the molecule, in both the closed (compact) state and the extended single-stranded form. This model is typically used to describe the statistical conformational properties of polymer chains in the long length regime: i.e. for $L_c \gg L_p$ (where L_c is the contour length and L_p is the persistence length of the molecule). In some cases, however, the WLC approximation has been successfully applied to depict the energy landscape of relatively short hairpin molecules (till about 5 to 6 bp stem).²

In our system, the end-to-end distance of the compact hairpin (R_{cl}) is approximately equal to the diameter of the double helical stem region (2 nm), whereas the fully extended duplex form reaches an end-to-end distance (R_{op}) of about 5.1 nm (due to formation of a 15 bp duplex segment with a helical rise of 0.34 nm/bp). We here assume that the end-to-end distance of the single-stranded form in our constructs is equal to R_{op} .

Thus, considering a persistence length for single-stranded DNA of 1.5 nm and a helical rise for ssDNA of 0.65 nm/base,³ one can calculate the entropic force experienced at the ends of the hairpin “spring” in both the closed ($F_{spring,cl}$) and extended ($F_{spring,op}$) form, applying Eq. 9 below

$$F_{spring} \approx \frac{k_B T}{L_p} \left(\frac{1}{4 \left(1 - \frac{R}{L_c}\right)^2} - \frac{1}{4} + \frac{R}{L_c} \right) \quad \text{Eq. 9}$$

where $k_B T$ is 4.1 pN nm and the contour length L_c of the 21 bases-long hairpin motif is 13.6 nm. The force contribution given by the unpaired M13mp18 scaffold segments on top (140 bases) and bottom (141 bases) of the DNA origami structure can be also calculated. In total, the force experienced at the ends of a *single* hairpin tethered to our DNA origami structure is 0.8 pN, in its closed configuration and 1.7 pN in its open single-stranded form. Thus, when summing up the contributions of 17 identical hairpin motifs aligned in parallel (see section 2), the overall entropic forces are, respectively, 11.3 pN for the closed form and 25.1 pN for the open single-stranded form.

The free energy stored in the entropic spring² in both states can be derived by integrating the force function of Eq. 9 from 0 to R (with R = R_{cl} or R_{op}), according to Eq. 10:

$$E_{spring} = \int_0^R F_{spring}(R)d(R) = \frac{k_B T L_C}{4L_p} \left(\frac{3(R/L_C)^2 - 2(R/L_C)^3}{(1 - R/L_C)} \right) \quad \text{Eq. 10}$$

Substituting with the parameters of our system and numerically solving, this leads to a difference in entropic conformational energy between the open and the closed state of a *single* hairpin motif ($\Delta G_{spring} = E_{spring, op} - E_{spring, cl}$) of 0.7 kcal mol⁻¹. The total energetic gap for 17 identical hairpins in parallel will be therefore 12.4 kcal mol⁻¹ (ΔG_{spring}). This is basically the WLC contribution to the unfolding of 17 hairpin motifs tethered in our construct I/5.

Summing up this WLC term with the thermodynamic NN term from base-pairing disruption ($\Delta G_{unfold} = 6.8$ kcal mol⁻¹) one obtains a theoretical value of 19.2 kcal mol⁻¹ for 17 hairpins organized together in parallel ($\Delta G_{teth} = \Delta G_{spring} + \Delta G_{unfold}$). This result agrees very well with the experimental value observed for I/5 (19.5 kcal mol⁻¹) strongly suggesting the validity of the approximation proposed.

We noticed that varying the “weight” of the scaffold contribution or other geometric parameters of our system leads to maximal deviations of ca. 13%, which are still fully acceptable. In addition, one should point out that the hybrid model proposed finds its better application for a fully tethered system, like for example the I/5 construct. Reducing the degree of tethering, that is, reducing the number of hairpins connected together and/or the structural rigidity of the surrounding microenvironment, compromises the reliable application of the WLC contribution due to a less defined end-to-end distance in the initial and final state of the molecules.

Alternative elastic model: the Freely Jointed Chain (FJC) model

In the freely jointed model, the polymer-like molecule is treated as a semi-flexible chain constituted by identical small segments jointed together by flexible hinges. In some cases, this model has been found more reliable for the description of the elastic properties of single-stranded DNA chains.^{4,5} We therefore tested whether application of the FJC model would lead to similar conclusions as the WLC model. In the FJC model the entropic force at the ends of the chain and the corresponding energy stored are described by the following equations:

$$F_{spring} = \frac{3k_B T}{2L_C L_p} R \quad \text{Eq. 11}$$

$$E_{spring} = \int_0^R F_{spring}(R) d(R) = \frac{3}{4} \left(\frac{k_B T R^2}{L_C L_p} \right) \quad \text{Eq. 12}$$

Substituting with the parameters described above for our system, we obtained a final elastic contribution (ΔG_{spring}) of 10.5 kcal mol⁻¹ for 17 identical hairpins in parallel, leading to a total ΔG_{teth} of 17.4 kcal mol⁻¹, which deviates only 10% from the experimentally observed value (19.5 kcal mol⁻¹). Also in this case, varying the contribution from the scaffold leads to maximal deviations of ca. 10-15%, which is still acceptable for approximated models.

Altogether, these theoretical considerations suggest that the elastic contribution from the entropic conformational energy of the tethered hairpins may indeed account for the increased unfolding energy observed.

4. Design of the tethered hairpin motifs

Two-dimensional DNA origami structures were designed as previously reported.⁶ All constructs analyzed are reported in Fig. S5-S7. To monitor the thermal as well as the conformational transition of the hairpins, two FRET reporters have been placed at facing positions of the seam as schematically illustrated in Fig. S8. Molecular models and energetic analysis of the DNA switchable motifs were created with the NUPACK package (<http://www.nupack.org>) as shown in Fig. S9-S11.

Construct II contains two identical sets of parallel hairpins, each 15 bases-long with sequence C₅T₅G₅. These are connected by a 12 bp long double helical segment. In this way, the total distance between the two halves of the origami device is about 4 helical turns, which ensures them to assume the same orientation in respect to the plane. The sequence of the inner segment has been designed using the NUPACK tool, such to be thermally stable at the conditions of fuel hybridization. Two sequences have been selected (segment A: ATCGAACTGGGC and segment B: CGCTGATGCACT, respectively indicated in Fig. S9a and b). The efficiency of device operation has been evaluated in both cases, imaging the biotin/streptavidin modified constructs with AFM (Fig. S17). The results showed better performance for segment B, which was then used for designing the seam of construct III (Fig. S10 and S11).

5. Temperature-dependent FRET spectroscopy

In the following we describe the procedure adopted for the thermal analysis of the device in its closed state, assuming that the thermal denaturation of the structure follows a two-state model (applied only in case the transition is cooperative and reversible). The folded fraction of the closed form θ_{cl} is related to the equilibrium constant of the closed state $K_{eq,cl}$ by the following formula:

$$K_{eq,cl} = \frac{[F_{cl}]}{[U_{cl}]} = \frac{\theta_{cl}}{1 - \theta_{cl}} \quad \text{Eq. 13}$$

The folded fraction is proportional to the FRET efficiency (E), which has been calculated by the donor-quenching method according to:

$$E = 1 - \frac{I_{DA}}{I_D} \quad \text{Eq. 14}$$

where I_{DA} and I_D correspond, respectively, to the fluorescence emission intensity of the donor (in our case, fluorescein) in presence and in absence of the acceptor.

Applying the van't Hoff equation to a restricted interval of temperatures near the melting temperature, the thermodynamic parameters of the transition can be extracted as follows:

$$K_{eq,cl} = e^{-\Delta G_{cl}/RT}$$
$$\ln K_{eq,cl} = -\frac{\Delta G_{cl}}{RT} = -\frac{\Delta H_{cl}}{R} \frac{1}{T} + \frac{\Delta S_{cl}}{R} \quad \text{Eq. 15}$$

The enthalpy and entropy change of the thermal transition for the closed state can be extracted, respectively, from the slope and intercept of the linear plot of the $\ln K_{eq,cl}$ versus $1/T$. Applying the same procedure to the open state and considering that the unfolded state is independent on the initial form of the system, being this either closed or open, one can in principle obtain the thermodynamic parameters associated to the structural reconfiguration

of the system (as described in the main text). A complete list of the data obtained by FRET thermal analysis is given in Table S1 and S2.

Note: A remarkable point concerns the trend observed for the melting temperatures. Although leading to similar conclusions as for the free energy changes, the variations in the T_m values were generally less pronounced (cfr. grey and black bars in Fig. 4a and b of the main text). In particular, one can note that structural differences located far away from the FRET labels were more easily revealed by variations in the ΔG (and ΔH) values (main text, Fig. 4a and b, grey bars; see also Tables S1 and S2). We explain this effect considering that the ΔH value of a thermal transition is derived by application of the van't Hoff equation to a restricted interval of temperatures near the T_m and is basically related to the slope of the melting/cooling profile in that region. Thus, whereas the melting temperature keeps mostly unaltered by the slope of the curve, this latter might be more sensitive to small variations in the structural properties of the sample (even at distant sites from the fluorescent labels), eventually yielding to distinct values of enthalpy and free energy change. Within the experimental errors, similar conclusions can be drawn by analysis of the FRET melting (rather than cooling) profiles of the closed forms (Table S2).

6. Temperature dependent UV spectroscopy

The assembly/disassembly of 40 μL of sample I/5 (2.5 nM scaffold, 12 nM staple strands and 5 nM dye modified strands) was monitored following the absorbance at 260 nm and varying the temperature from 80°C to 20°C, at a rate of ± 0.1 °C/min, using an UV-Vis spectrophotometer (Cary 300 BIO UV-Visible Spectrophotometer, Varian Inc.). A quartz UV microcuvette (#6610024200, Agilent Technologies, 40 μL , 1 cm) was used at this purpose. Three independent runs were performed (one representative is shown in Fig. S13). The fit has been calculated applying a sigmoidal Boltzmann equation as provided by the Origin v.7 software (MicroCal).

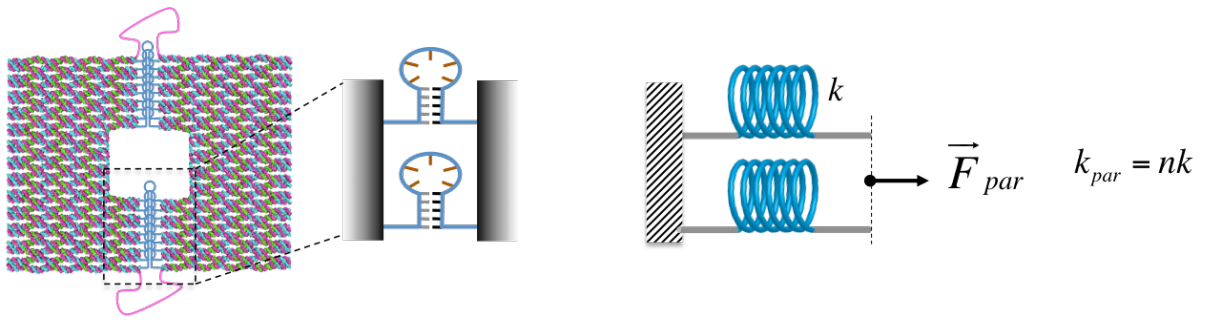


Fig. S2. Schematic illustration of two hairpin motifs in parallel. Approximating each hairpin as a spring element, the mechanical properties of the two-spring system will be equal to those of a single spring with an additive spring constant.

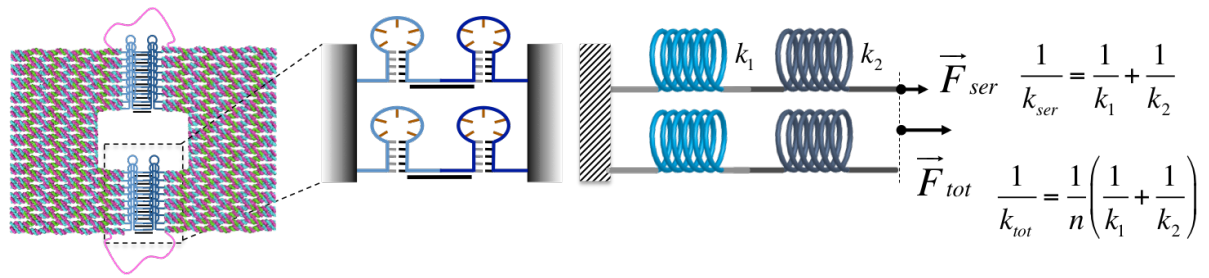


Fig. S3. Schematic illustration of two different sets of parallel hairpin motifs in series. Applying the spring model to each hairpin element allows to calculate the elastic properties of the ensemble of springs.

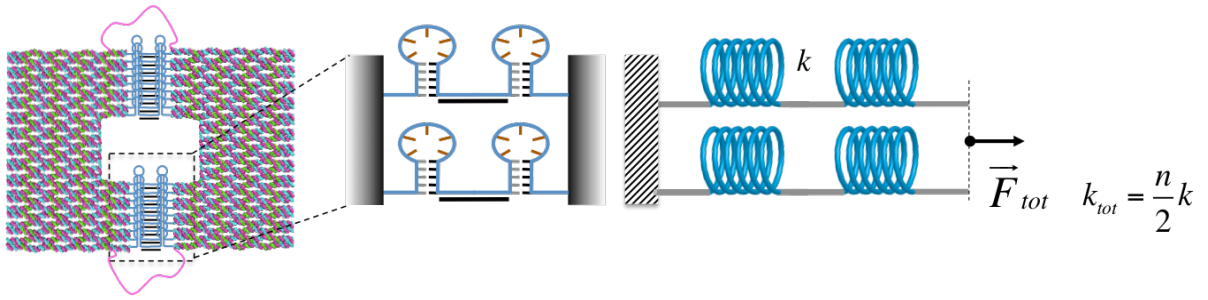


Fig. S4. Schematic illustration of two identical sets of parallel hairpin motifs in series. When the two sets of springs have the same spring constant, the mechanical properties of the system simplify.

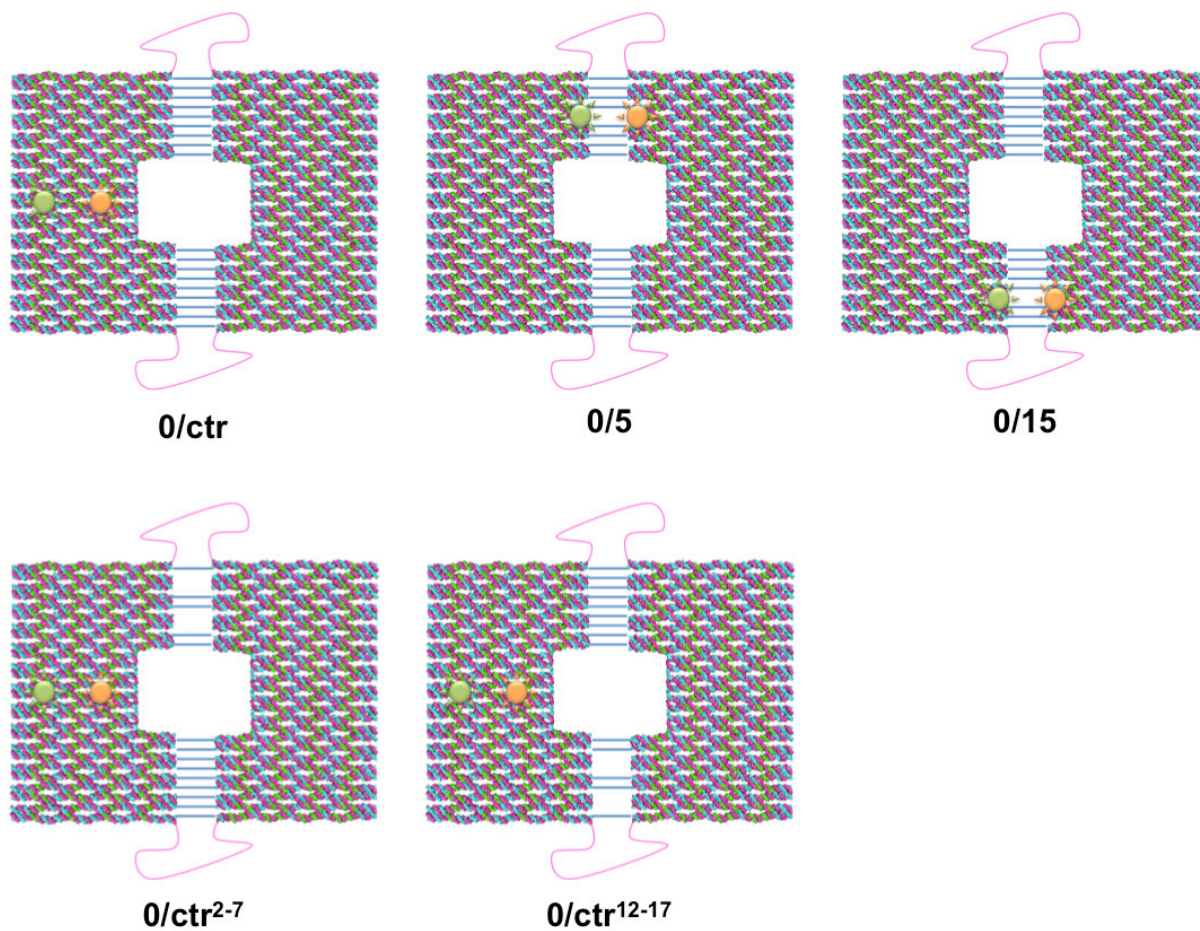


Fig. S5. Different types of constructs type 0 analyzed in this work. Such a system bears no hairpins in the central seam. FRET reporters were embedded either within the origami structure in the center of the left-side region (0/ctr) or within the seam, at position 5 (0/5) or 15 (0/15). Control samples lacking seam staples at positions 2 to 7 (0/ctr²⁻⁷) or 12-17 (0/ctr¹²⁻¹⁷) have been also analyzed.

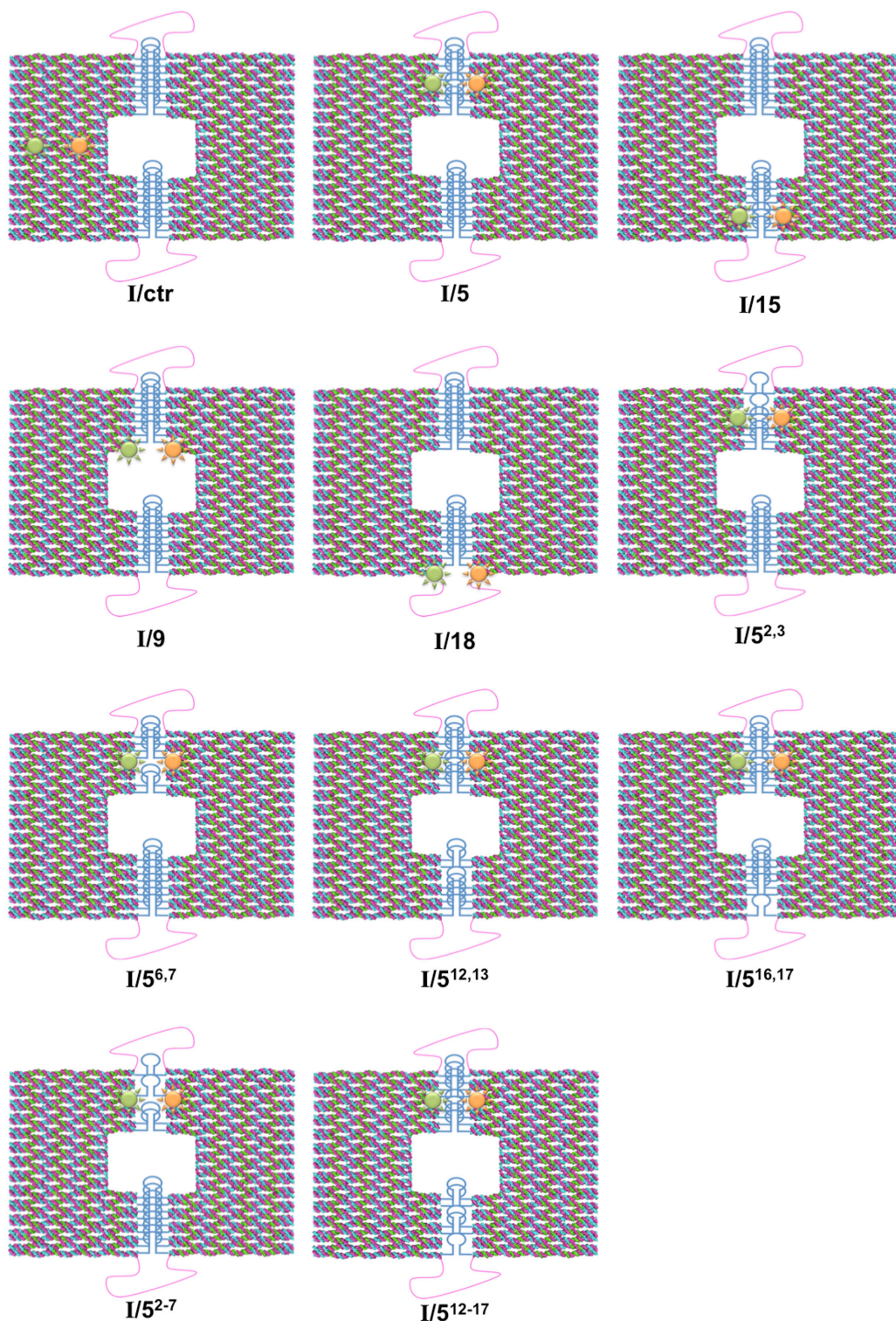


Fig. S6. Construct type I bears one set of parallel hairpin loops in the central seam. Details on the design are reported elsewhere.⁶ FRET reporters were embedded either within the origami structure in the center of the left-side region (I/ctr) or within the seam, at position 5 (I/5), 15 (I/15), 9 (I/9) or 18 (I/18). A detail of the labeling strategy adopted is reported in Fig. S8 for the I/5 sample. An additional set of I/5 samples was also analyzed, lacking two seam staples either at positions 2,3 (I/5^{2,3}), 6,7 (I/5^{6,7}), 12,13 (I/5^{12,13}) or 16,17 (I/5^{16,17}). In addition, samples lacking four seam staples were also prepared, either at positions 2 to 7 (I/5²⁻⁷) or 12 to 17 (I/5¹²⁻¹⁷).

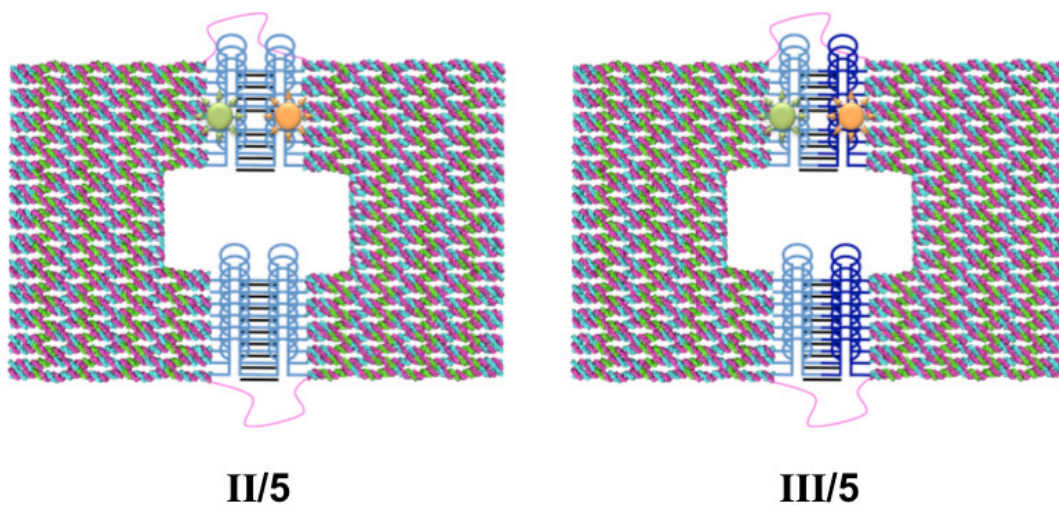


Fig. S7. Constructs type II and III bear, respectively, two identical and two different sets of parallel hairpin motifs in the central seam of the structure (details of the design are reported below in Fig. S9). FRET reporters have been placed at position 5 in both constructs (II/5 and III/5).

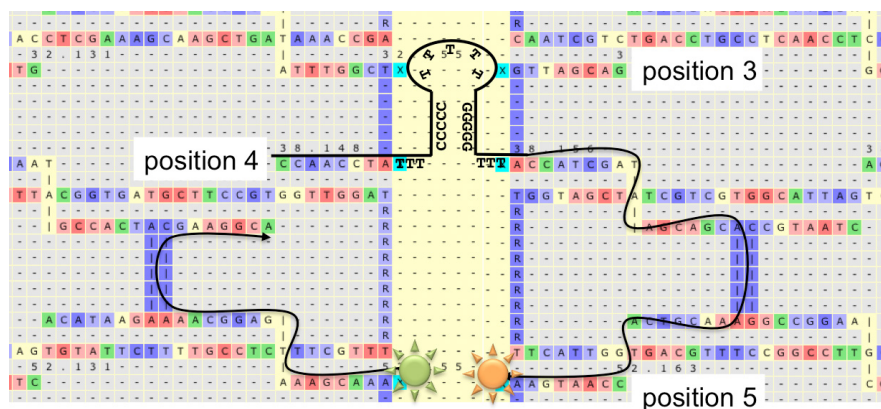


Fig. S8. Detailed view of the labeling strategy adopted to monitor the FRET change during assembly/disassembly of the structure at the central seam (i.e. thermal transition), as well as during the conformational transition of the hairpin motif from its compact (high FRET) to extended (low FRET) state upon addition of complementary fuel strands. Note that using this design, FRET changes can be monitored only in conjunction with correct formation of the hairpin motifs and their integration into the origami structure, thus excluding any signal contribution from formation of free hairpins in solution.

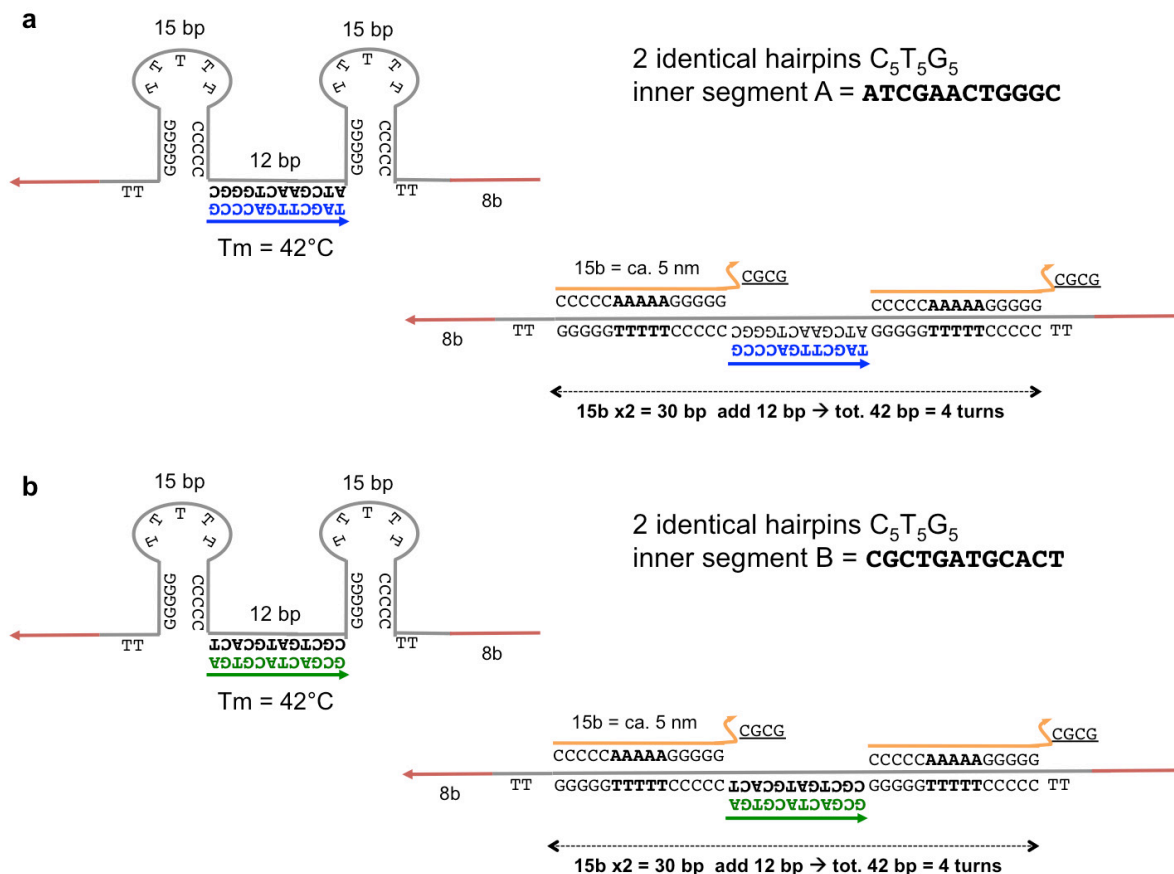


Fig. S9. Design of the hairpin motifs for construct II. The sequences of the hairpins and corresponding fuel strands are as previously reported.⁶ The double helical segment connecting the two hairpins has been designed using the NUPACK package (see section 4 above). Two possible sequences have been selected: segment A (**a**) and segment B (**b**). Segment B gave the best results of device performance (Fig. S17), therefore it was chosen for the construct III (Fig. S10 and S11).

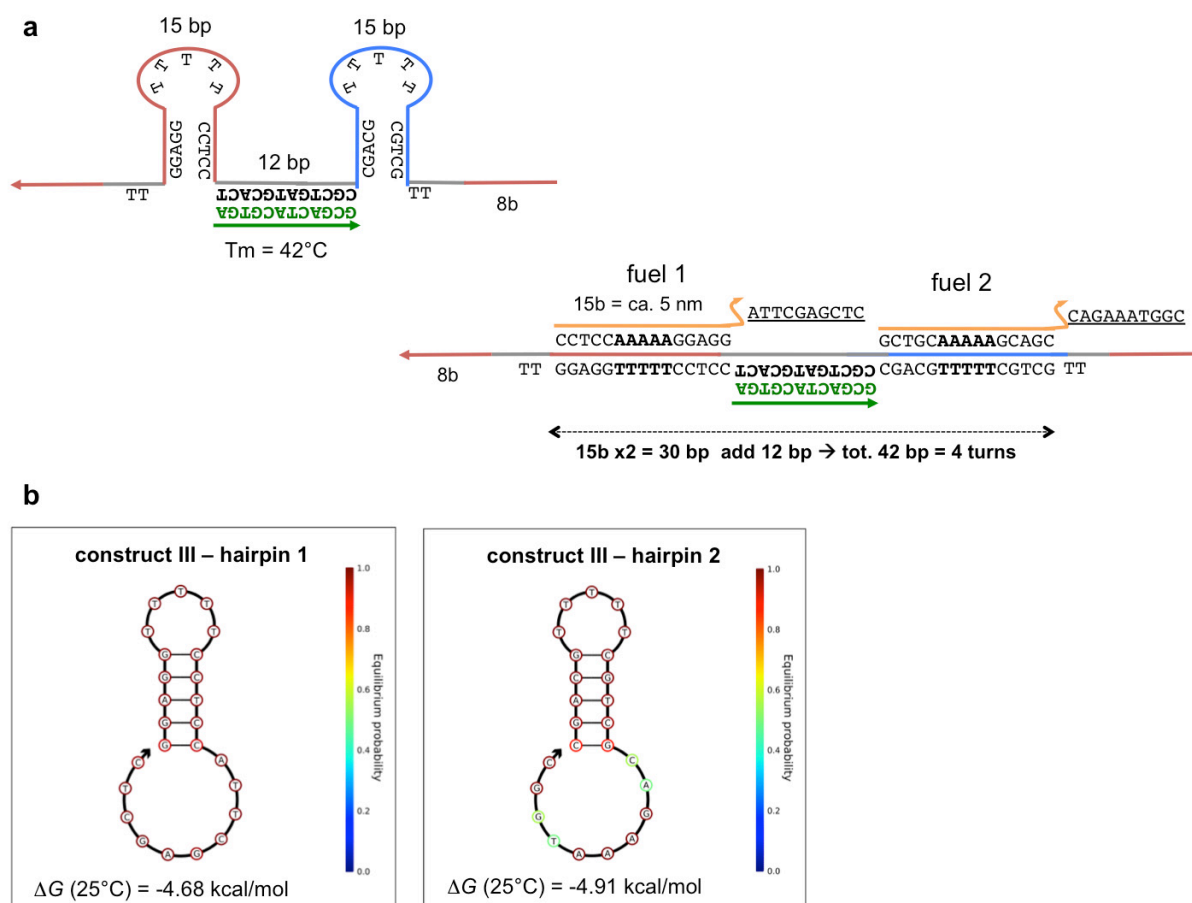


Fig. S11. Design of the seam sequences of construct III (**a**): these are two different hairpin motifs that can be actuated by two distinct fuels/antifuels strands, thus allowing independent cycles of extension/contraction movements. In (**b**) are the models generated by the NUPACK software. The values of free energy change at 25°C indicate that the motifs are stable at room temperature and that their thermal stability is approximately equal.

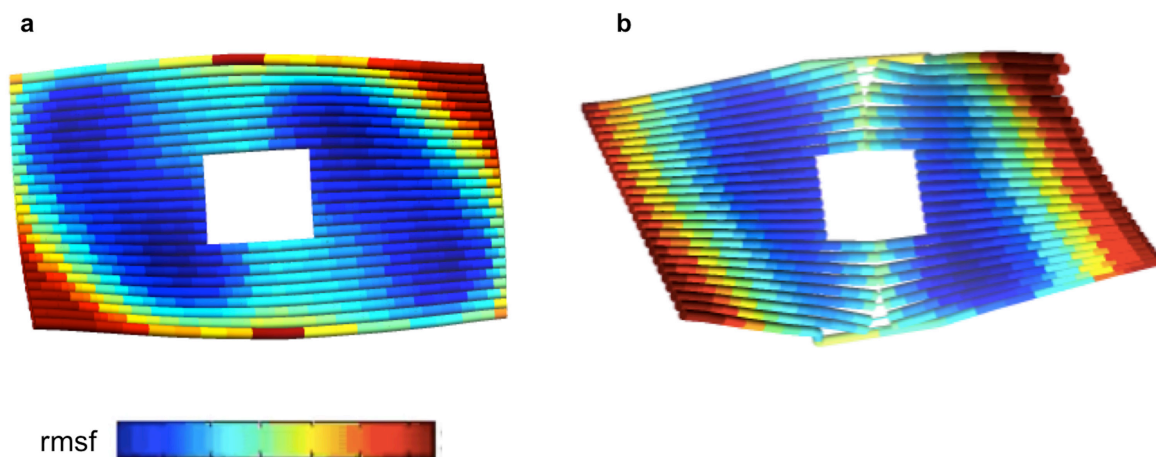


Fig. S12. 3D geometric model of the DNA origami structure lacking (a) or bearing (b) single-stranded segments in the central seam. The models have been obtained by the CanDo software tool (<https://cando-dna-origami.org>) and map the structural flexibility of the molecule in color code using standard geometric parameters of the DNA helical structure.¹⁰ The geometric flexibility of the structure is expressed as rmsf (root mean square flexibility), from a minimal (blue) to a maximal relative value (red). The seam in (b) was modified with 21 bases-long single-stranded DNA segments, to emulate the presence of hairpins. The results indicate that although the two structures have different global flexibilities, these are symmetrically distributed around the seam in both cases. That is, the disparity in the thermal stability observed between the upper and lower region of the DNA origami structure cannot be attributed to distinct geometric environments, rather appears to be dependent from differences in base content.

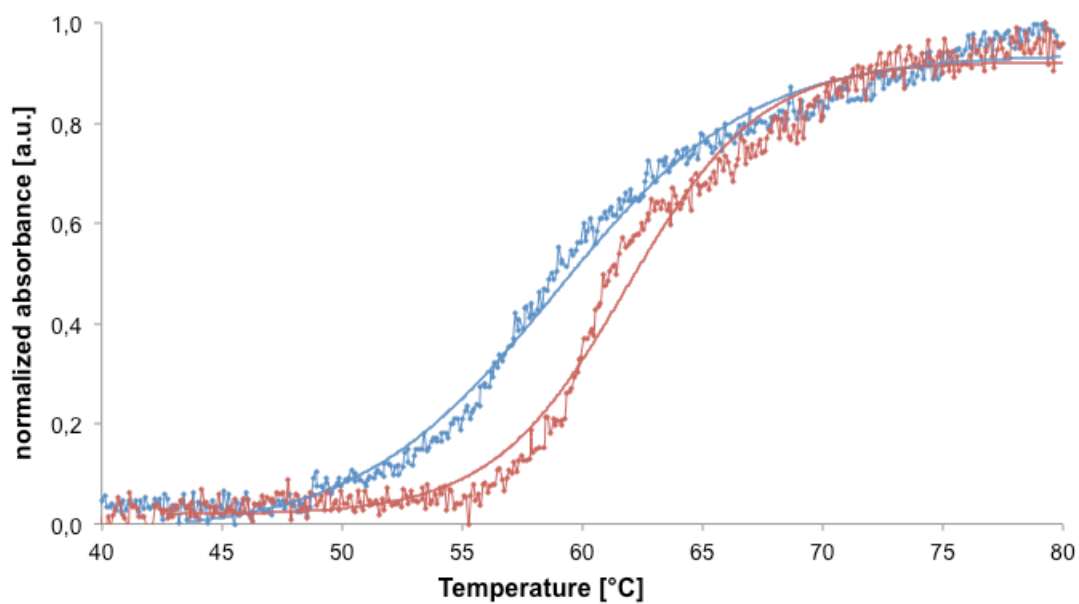


Fig. S13. Representative cooling (*blue*) and melting (*red*) profile of the 1/5 sample monitored by UV spectroscopy. The hysteresis of the process indicates the (global) non-reversibility of the thermal transition. This is quite expected, as DNA origami structures display sequence-dependent regions of different thermal stability.¹¹

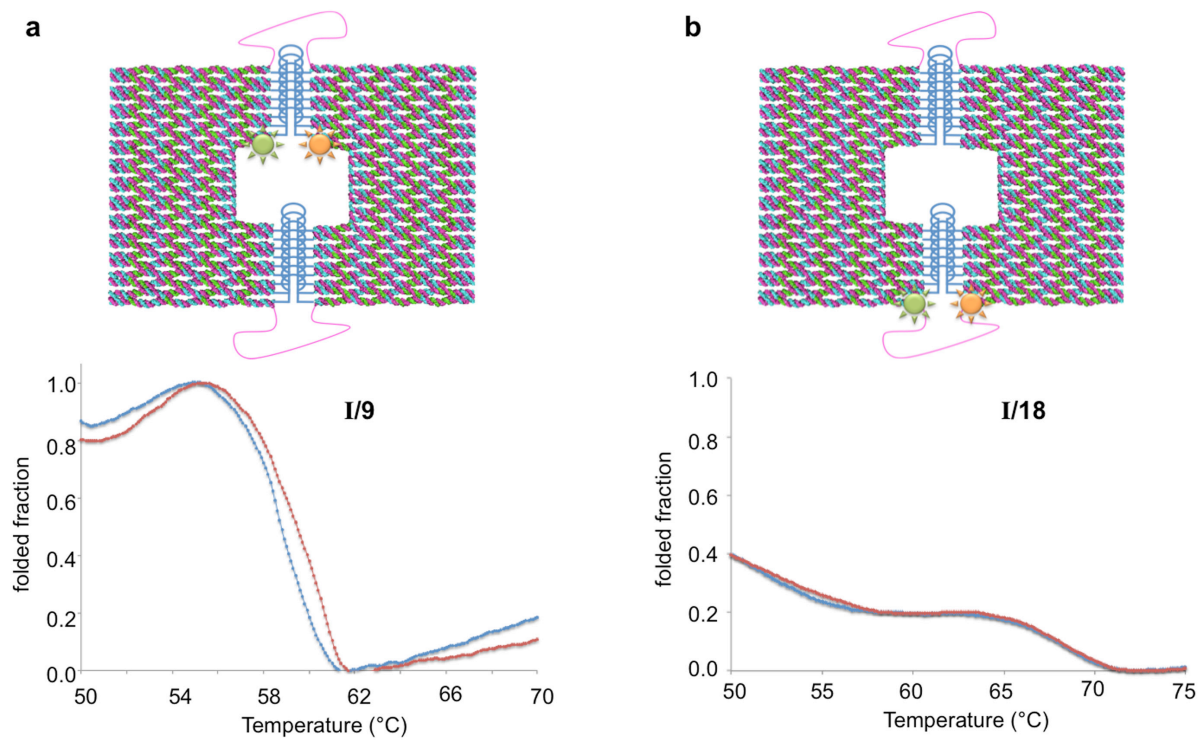


Fig. S14. Normalized FRET cooling (*blue curves*) and melting (*red curves*) profiles obtained for constructs I/9 (**a**) and I/18 (**b**). In both cases, the curves are not suitable for application of the van't Hoff analysis as they present either thermal hysteresis (a) or a monotonic transition (b). In these constructs, the fluorescent labels were positioned respectively on the inner or outer edges of the structures, thus providing only a limited anchoring surface and preventing the clear manifestation and/or visualization of the scaffolding effect.

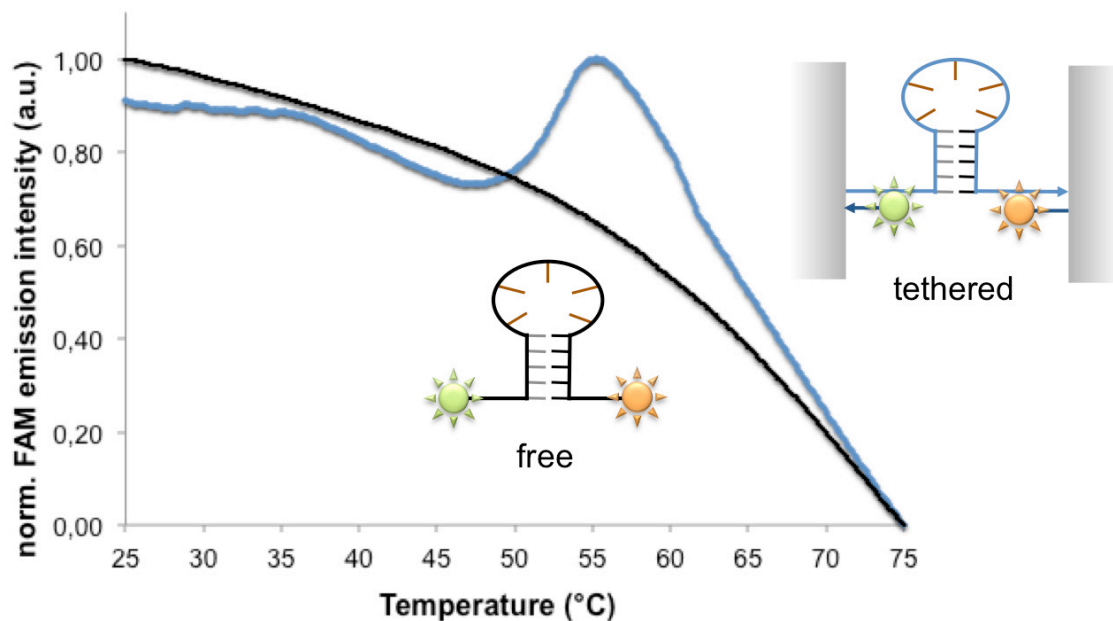


Fig. S15. Normalized FAM emission intensity during the cooling process of a doubly labeled hairpin motif ($C_5T_5G_5$), either free in solution (*black curve*) or tethered to an origami surface at position 5 of the seam (*blue curve*, corresponding to the construct I/5). Clearly, tethering of the motif to the origami structure allows for the thermal transition to be visible (around 53 °C), indicating that tight anchoring to a large and compact structure provides sufficient rigidity to keep the distance between the fluorescent labels well defined. This is indeed not verified for the same motif free in solution. Although the measured value of thermal stability of the fully tethered hairpin is about only three-fold higher than the expected value for the same motor freely moving in solution, these data demonstrate that such a small difference is indeed sufficient for visualization of the process even at nanomolar concentrations.

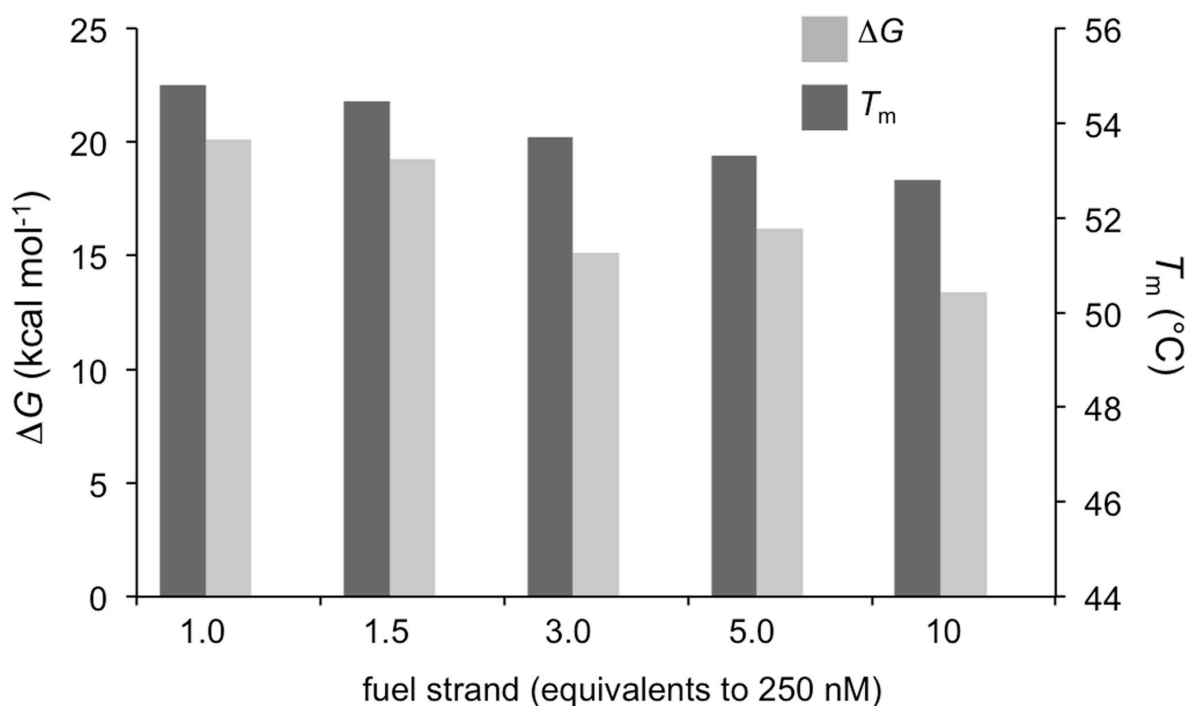


Fig. S16. Free energy changes at 25°C (*grey bars*) and melting temperatures (*black bars*) for the melting process of construct I/5 in its duplex form and in presence of different equimolar amounts of fuel strand (from 0.25 mM to 2.5 mM). The results indicate that *increasing* fuel concentration, both the free energy change of duplex denaturation and the melting temperature *decrease*. This implies that the enhanced thermal stability observed by tethering multiple motifs in parallel cannot be attributed to an increased local concentration of fuel molecules in the direct proximity of the duplexes. The whole energy landscape of the system reveals to be rather complex and dependent from many experimental and design parameters. Nevertheless, the general trend observed for both the closed (hairpin) constructs and the open (duplex) constructs holds true: that is, the higher the degree of hairpin tethering, the higher its thermal stability.

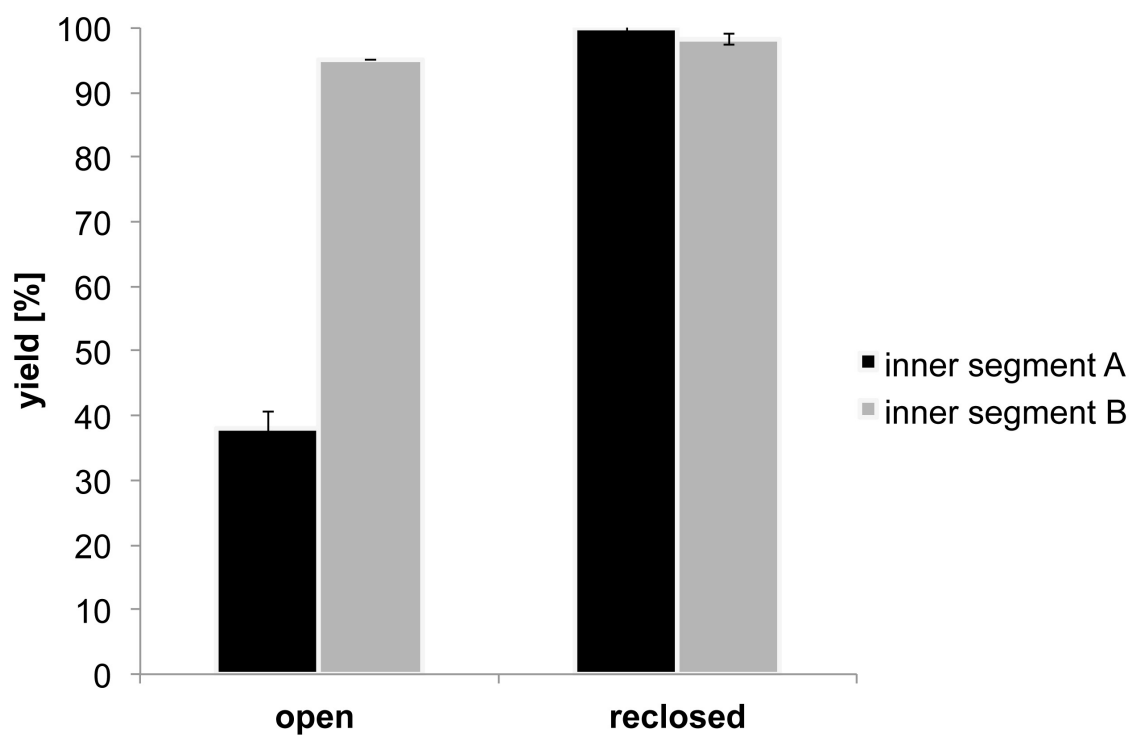


Fig. S17. AFM-based statistical analysis of the efficiency of the opening and reclosing process for construct II, containing either segment A (*black bars*) or segment B (*grey bars*) as bridge between the two consecutive and identical hairpin motifs. Although the reclosing process is almost quantitative for both designs, the opening process was much more efficient for design B. This was then used to design construct III.

Table S1. Thermodynamic parameters obtained from temperature-dependent FRET experiments for the cooling process. Only samples giving reversible and cooperative thermal transitions were treated by the van't Hoff analysis, allowing to extract the values of melting temperature (T_m) enthalpy (ΔH), entropy (ΔS) and free energy change at 25 °C ($\Delta G^{25^\circ\text{C}}$). The number of hairpin motifs inserted within the seam of the origami structure is also indicated (n°).

n°	name	COOLING							
		closed				open			
		T_m	ΔH	ΔS	$\Delta G^{25^\circ\text{C}}$	T_m	ΔH	ΔS	$\Delta G^{25^\circ\text{C}}$
17	I/5	52.2±0.1	-58±2	-0.26±0.01	19.5	52.0±0.2	-66 ± 8	-0.30±0.04	23.4
17	I/9	58.8±0.1	--	--	--	58.6±0.1	--	--	--
17	I/15	48.7±0.3	-52±7	-0.23±0.04	16.6	49.0±0.3	-51±10	-0.23±0.04	17.5
17	I/18	--	--	--	--	--	--	--	--
18	I/CTR	58.4±0.03	-182±3	-0.85±0.02	71.4	58.1±0.1	-193±6	-0.90±0.02	75.3
13	I/5 ²⁻⁷	48.8±0.1	-26±2	-0.12±0.01	9.8	50.5±0.1	-28.0±0.4	-0.13±0.01	10.7
14	O/ctr ²⁻⁷	58.4±0.1	-193±19	-0.9±0.1	75.3	58.4±0.1	-151±6	-0.70±0.03	57.7
13	I/5 ¹²⁻¹⁷	51.3±0.1	-37±1	-0.17±0.01	13.7	52.2±0.1	-39±2	-0.18±0.01	14.6
14	O/ctr ¹²⁻¹⁷	58.3±0.1	-166.5±0.4	-0.70±0.10	42.2	58.4±0.1	-149±6	-0.69±0.03	56.7
15	I/5 ^{2,3}	50.7±0.2	-35±3	-0.16±0.01	12.7	51.5±0.3	-55±6	-0.25±0.03	19.5
15	I/5 ^{6,7}	50.9±0.3	-33±4	-0.15±0.02	11.7	51.1±0.5	-40±1	-0.18±0.01	13.6
15	I/5 ^{12,13}	54.1±0.1	-50±3	-0.23±0.01	18.6	54.3±0.1	-67±4	-0.31±0.02	25.4
15	I/5 ^{16,17}	54.7±0.1	-68±5	-0.31±0.02	24.4	54.5±0.1	-74±1	-0.34±0.01	27.3
0	O/5	58.1±0.1	-128±2	-0.60±0.01	50.9	--	--	--	--
0	O/15	52.7±0.1	-62±3	-0.28±0.01	21.5	--	--	--	--
0	O/ctr	58.5±0.1	-207±5	-0.97±0.02	82.2	--	--	--	--
34	II/5	46.5±0.6	-28±8	-0.12±0.03	7.8	--	--	--	--
34	III/5	47.6±0.2	-32±1	-0.14±0.01	9.7	--	--	--	--

Table S2. Thermodynamic parameters obtained from temperature-dependent FRET experiments for the melting process. Only samples giving reversible and cooperative thermal transitions were treated by the van't Hoff analysis, allowing to extract the values of melting temperature (T_m) enthalpy (ΔH), entropy (ΔS) and free energy change at 25 °C ($\Delta G^{25^\circ\text{C}}$). The number of hairpin motifs inserted within the seam of the origami structure is also indicated (n°).

n°	name	MELTING							
		closed				open			
		T_m	ΔH	ΔS	$\Delta G^{25^\circ\text{C}}$	T_m	ΔH	ΔS	$\Delta G^{25^\circ\text{C}}$
17	I/5	52.9±0.1	65±2	0.29±0.01	-21.5	52.9±0.1	70±3	0.32±0.02	-25.4
17	I/9	59.5±0.1	--	--	--	59.6±0.1	--	--	--
17	I/15	48.4±0.1	50±7	0.22±0.03	-15.6	49.2±0.2	48±2	0.21±0.01	-14.6
17	I/18	--	--	--	--	--	--	--	--
18	I/CTR	59.5±0.1	267±6	1.25±0.03	-105.7	59.4±0.1	262±2	1.23±0.01	-104.7
13	I/5 ²⁻⁷	49.7±0.1	28.6±0.3	0.13±0.01	-10.2	51±0.3	30±2	0.14±0.01	-11.7
14	O/ctr ²⁻⁷	59.6±0.1	193±11	0.91±0.05	-78.3	59.8±0.1	233±2	1.10±0.01	-95.0
13	I/5 ¹²⁻¹⁷	52.2±0.1	48±2	0.22±0.10	-17.6	52.2±0.2	54±11	0.24±0.05	-17.6
14	O/ctr ¹²⁻¹⁷	59.6±0.1	176±2	0.83±0.01	-71.5	59.7±0.1	229±3	1.08±0.03	-93.0
15	I/5 ^{2,3}	52.7±0.08	67±1	0.30±0.01	-22.4	52.3±0.4	55±12	0.25±0.05	-19.5
15	I/5 ^{6,7}	52.0±0.2	41±2	0.18±0.01	-12.7	51.7±0.5	36±5	0.16±0.03	-11.7
15	I/5 ^{12,13}	55.2±0.03	69±1	0.32±0.01	-26.4	54.8±0.2	76±6	0.35±0.03	-28.4
15	I/5 ^{16,17}	55.9±0.08	84±8	0.38±0.04	-29.3	56.1±0.1	64±4	0.29±0.02	-22.5
0	O/5	60.0±0.1	125±8	0.59±0.04	-50.9	--	--	--	--
0	O/15	53.6±0.1	53±1	0.24±0.01	-18.6	--	--	--	--
0	O/ctr	59.6±0.1	249±3	1.17±0.02	-99.8	--	--	--	--
34	II/5	47.6±0.5	30±10	0.13±0.05	-8.8	--	--	--	--
34	III/5	49.0±0.2	39±1	0.17±0.01	-11.7	--	--	--	--

Table S3. List of the oligonucleotides used for FRET analysis of the hairpin motifs of construct I.

n°	Oligoname	Sequence (5'- 3')
4	loop4-TAMRA	CCAACCTATTTCCCCTTTTTGGGGTTTACCATCGATAGCAGCAAACG TCACCAATGAA-TAMRA
5	FAM-loop5	FAM-AAACGAAAGAGGCAAACGAAGGCA
8	loop8-TAMRA	CGCCAAAATTTCCCCTTTTTGGGGTTTAAAACAGGGAAGCGCACG AGAGAATAACAT-TAMRA
9	FAM-loop9	FAM-GGAATTACGAGGCATAATACATAA
14	loop14-TAMRA	AACATACGTTTCCCCTTTTTGGGGTTTCAAATGAAAATCTAACGCT GAGAGCCAGCAG-TAMRA
15	FAM-loop15	FAM-AGCCGGAAGCATAAAGTTCCACAC
--	FAM_G138,52	FAM-GAAAAGGTGGAACGAGTAGATTTACCTTTTGA
--	G158,52_TAMRA	CCTGAGTAATGACCCTGTAATACTCGCGAGCT-TAMRA
18R	TAMRA-loop18_right	TAMRA-CGTTAGAATCAGAGCGGGAGCTAA
18L	loop18_left-FAM	CCCTTATAAAGCCGCGAACGTGGCGAGAAAGGAAGGGAA-FAM
4	no_loop4-TAMRA	CCAACCTAACCATCGATAGCAGCAAACGTCACCAATGAA-TAMRA
14	no_loop14-TAMRA	AACATACGCAAATGAAAATCTAACGCTGAGAGCCAGCAG-TAMRA

Table S4. List of the oligonucleotides used for FRET analysis of the hairpin motifs of construct II and III.

n°	Oligoname	Sequence (5' - 3')
4	loop4-2i-B-TAMRA	CCAACCTATCCCCCTTTTTGGGGGCGCTGATGCACTCCCCCTTTTTGG GGTTACCATCGATAGCAGCAAACGTCACCAATGAA-TAMRA
4	loop4-2d-B-TAMRA	CCAACCTATTGCTGCTTTTTGCAGCCGCTGATGCACTCCTCCTTTTTGGA GGTTACCATCGATAGCAGCAAACGTCACCAATGAA-TAMRA
5	FAM-loop5	FAM-AAACGAAAGAGGCAAACGAAGGCA

Table S5. List of the oligonucleotides used for modification of the seam in construct I.

n°	Oligoname	Sequence (5'- 3')
2	LG18,148P	TAATTGTATTTCCCCCTTTTTGGGGGTTTGCCTTGATATTCACAAGCAGGTCA
4	LG38,148P	CCAACCTATTTCCCCCTTTTTGGGGGTTTACCATCGATAGCAGCAAAACGTCA
6	LG58,148P	TTCATTACTTTCCCCCTTTTTGGGGGTTTAAACGTAGAAAATACATACGCAGT
8	LG78,148P	CGCCAAAATTTCCCCCTTTTTGGGGGTTTAAAAACAGGGAAGCGCACAGAGAG
10	LG178,148P	AATTTTTGTTTCCCCCTTTTTGGGGGTTTTTTCAATTACCTGAGCAGAGGCGA
12	LG198,148P	ACCAGGCATTTCCCCCTTTTTGGGGGTTTCACCAGAAGGAGCGGATGCCGAAC
14	LG218,148P	AACATACGTTTCCCCCTTTTTGGGGGTTTCAAATGAAAAATCTAACGCTGAGA
16	LG238,148P	CTGTTTGATTTCCCCCTTTTTGGGGGTTTGCTCAATCGTCTGAAAATACCTAC
18	LG258,148P	GAAGGGAATTTCCCCCTTTTTGGGGGTTTCGTTAGAATCAGAGCGGGAGCTAA
1	LG12,163P	GGCGGATATTTCCCCCTTTTTGGGGGTTTCAAGCCAATAGGAACCCATGTAC
3	LG32,163P	GACGATTGTTTCCCCCTTTTTGGGGGTTTTCGGTTTATCAGCTTGGGAGCCTT
5	LG52,163P	CCAATGAATTTCCCCCTTTTTGGGGGTTTAAACGAAAGAGGCAAACGAAGGCA
7	LG72,163P	ATGTTAGCTTTCCCCCTTTTTGGGGGTTTCAAATCAACGTAACAACCGGATA
9	LG92,163P	AATAACATTTTCCCCCTTTTTGGGGGTTTGAATTACGAGGCATAATACATAA
11	LG192,163P	ATTATTCATTTCCCCCTTTTTGGGGGTTTTTAAATCAGCTCATTTTCGCATTA
13	LG212,163P	AAAGAAACTTTCCCCCTTTTTGGGGGTTTAAGCGCCATTCGCCATTGCCGGAA
15	LG232,163P	GCCAGCAGTTTCCCCCTTTTTGGGGGTTTAGCCGGAAGCATAAAGTTCCACAC
17	LG252,163P	ATTTTGACTTTCCCCCTTTTTGGGGGTTTGGTGGTTCCGAAATCCGAAAATC

Table S6. List of the oligonucleotides used for modification of the seam in construct II with inner sequence A: ATCGAACTGGGC.

n°	Oligoname	Sequence (5'-3')
2	2ILA-1	TAATTGTATTCCCCCTTTTTGGGGGATCGAACTGGGCCCCCCTTTTTGGGGGTTGC CTTGATATTCACAAGCAGGTCA
4	2ILA-2	CCAACCTATTCCCCCTTTTTGGGGGATCGAACTGGGCCCCCCTTTTTGGGGGTTAC CATCGATAGCAGCAAACGTCA
6	2ILA-3	TTCATTACTTCCCCCTTTTTGGGGGATCGAACTGGGCCCCCCTTTTTGGGGGTTAAA CGTAGAAAATACATACGCAGT
8	2ILA-4	CGCCAAAATTCCCCCTTTTTGGGGGATCGAACTGGGCCCCCCTTTTTGGGGGTTAA AAACAGGGAAGCGCACAGAGAG
10	2ILA-5	AATTTTTGTTCCCCCTTTTTGGGGGATCGAACTGGGCCCCCCTTTTTGGGGGTTTTT CAATTACCTGAGCAGAGGCGA
12	2ILA-6	ACCAGGCATTCCCCCTTTTTGGGGGATCGAACTGGGCCCCCCTTTTTGGGGGTTCA CCAGAAGGAGCGGATGCGGAAC
14	2ILA-7	AACATACGTTCCCCCTTTTTGGGGGATCGAACTGGGCCCCCCTTTTTGGGGGTTCA AATGAAAAATCTAACGCTGAGA
16	2ILA-8	CTGTTTGATTCCCCCTTTTTGGGGGATCGAACTGGGCCCCCCTTTTTGGGGGTTGC TCAATCGTCTGAAAATACCTAC
18	2ILA-9	GAAGGGAATTCCCCCTTTTTGGGGGATCGAACTGGGCCCCCCTTTTTGGGGGTTCCG TTAGAATCAGAGCGGGAGCTAA
1	2ILA-10	GGCGGATATTCCCCCTTTTTGGGGGATCGAACTGGGCCCCCCTTTTTGGGGGTTCA AGCCCAATAGGAACCCATGTAC
3	2ILA-11	GACGATTGTTCCCCCTTTTTGGGGGATCGAACTGGGCCCCCCTTTTTGGGGGTTTC GGTTTATCAGCTTGGGAGCCTT
5	2ILA-12	CCAATGAATTCCCCCTTTTTGGGGGATCGAACTGGGCCCCCCTTTTTGGGGGTTAA ACGAAAGAGGCAAACGAAGGCA
7	2ILA-13	ATGTTAGCTTCCCCCTTTTTGGGGGATCGAACTGGGCCCCCCTTTTTGGGGGTTCC AAATCAACGTAACAACCGGATA
9	2ILA-14	AATAACATTTCCCCCTTTTTGGGGGATCGAACTGGGCCCCCCTTTTTGGGGGTTGG AATTACGAGGCATAATACATAA
11	2ILA-15	ATTATTCATTCCCCCTTTTTGGGGGATCGAACTGGGCCCCCCTTTTTGGGGGTTTTA AATCAGCTCATTTTCGCATTA
13	2ILA-16	AAAGAACTTCCCCCTTTTTGGGGGATCGAACTGGGCCCCCCTTTTTGGGGGTTAA GCGCCATTCGCCATTGCCGGAA
15	2ILA-17	GCCAGCAGTTCCCCCTTTTTGGGGGATCGAACTGGGCCCCCCTTTTTGGGGGTTAG CCGGAAGCATAAAGTTCCACAC
17	2ILA-18	ATTTTGACTTCCCCCTTTTTGGGGGATCGAACTGGGCCCCCCTTTTTGGGGGTTTG GTGGTCCGAAATCCGAAAATC

Inner sequence A: GCCCAGTTCGAT

Fuel: C₅A₅G₅CGCG; Antifuel: CGCGC₅T₅G₅

Table S7. List of the oligonucleotides used for modification of the seam in construct II with inner sequence B: AGTGCATCAGCG.

n°	Oligoname	Sequence (5'- 3')
2	2ILB-1	TAATTGTATTCCCCCTTTTTGGGGGCGCTGATGCACTCCCCCTTTTTGGGGGTTGCCT TGATATTCACAAGCAGGTCA
4	2ILB-2	CCAACCTATTCCCCCTTTTTGGGGGCGCTGATGCACTCCCCCTTTTTGGGGGTTACC ATCGATAGCAGCAAAACGTCA
6	2ILB-3	TTCATTACTTCCCCCTTTTTGGGGGCGCTGATGCACTCCCCCTTTTTGGGGGTTAAAC GTAGAAAATACATACGCAGT
8	2ILB-4	CGCCAAAATTCCCCCTTTTTGGGGGCGCTGATGCACTCCCCCTTTTTGGGGGTTAAA AACAGGGAAGCGCACAGAGAG
10	2ILB-5	AATTTTTGTTCCCCCTTTTTGGGGGCGCTGATGCACTCCCCCTTTTTGGGGGTTTTTC AATTACCTGAGCAGAGGCGA
12	2ILB-6	ACCAGGCATTCCCCCTTTTTGGGGGCGCTGATGCACTCCCCCTTTTTGGGGGTTTAC CAGAAGGAGCGGATGCGGAAC
14	2ILB-7	AACATACGTTCCCCCTTTTTGGGGGCGCTGATGCACTCCCCCTTTTTGGGGGTTCAA TGAAAAATCTAACGCTGAGA
16	2ILB-8	CTGTTTGATTCCCCCTTTTTGGGGGCGCTGATGCACTCCCCCTTTTTGGGGGTTGCTC AATCGTCTGAAAATACCTAC
18	2ILB-9	GAAGGGAATTCCCCCTTTTTGGGGGCGCTGATGCACTCCCCCTTTTTGGGGGTTTCG TAGAATCAGAGCGGGAGCTAA
1	2ILB-10	GGCGGATATTCCCCCTTTTTGGGGGCGCTGATGCACTCCCCCTTTTTGGGGGTTCAA GCCCAATAGGAACCCATGTAC
3	2ILB-11	GACGATTGTTCCCCCTTTTTGGGGGCGCTGATGCACTCCCCCTTTTTGGGGGTTTCG GTTTATCAGCTTGGGAGCCTT
5	2ILB-12	CCAATGAATTCCCCCTTTTTGGGGGCGCTGATGCACTCCCCCTTTTTGGGGGTTAAAC GAAAGAGGCAAACGAAGGCA
7	2ILB-13	ATGTTAGCTTCCCCCTTTTTGGGGGCGCTGATGCACTCCCCCTTTTTGGGGGTTCCAA ATCAACGTAACAACCGGATA
9	2ILB-14	AATAACATTTCCCCCTTTTTGGGGGCGCTGATGCACTCCCCCTTTTTGGGGGTTGGAA TTACGAGGCATAATACATAA
11	2ILB-15	ATTATTCATTCCCCCTTTTTGGGGGCGCTGATGCACTCCCCCTTTTTGGGGGTTTTAA ATCAGCTCATTTTCGCATTA
13	2ILB-16	AAAGAAACTTCCCCCTTTTTGGGGGCGCTGATGCACTCCCCCTTTTTGGGGGTTAAG CGCCATTCGCCATTGCCGGAA
15	2ILB-17	GCCAGCAGTTCCCCCTTTTTGGGGGCGCTGATGCACTCCCCCTTTTTGGGGGTTAGC CGGAAGCATAAAGTTCCACAC
17	2ILB-18	ATTTTGACTTCCCCCTTTTTGGGGGCGCTGATGCACTCCCCCTTTTTGGGGGTTTGGT GGTTCGAAATCCGAAAATC

Inner sequence B: AGTGCATCAGCG

Fuel: C₅A₅G₅CGCG; Antifuel: CGCGC₅T₅G₅

Table S8. List of the oligonucleotides used for modification of the seam in construct III with inner sequence B: AGTGCATCAGCG.

n°	Oligoname	Sequence (5'- 3')
2	2DLB-1	TAATTGTATTGCTGCTTTTTGCAGCCGCTGATGCACTCCTCCTTTTTGGAGGTTGCC TTGATATTCACAAGCAGGTCA
4	2DLB-2	CCAACCTATTGCTGCTTTTTGCAGCCGCTGATGCACTCCTCCTTTTTGGAGGTTACC ATCGATAGCAGCAAAACGTCA
6	2DLB-3	TTCATTACTTGCTGCTTTTTGCAGCCGCTGATGCACTCCTCCTTTTTGGAGGTTAAA CGTAGAAAATACATACGCAGT
8	2DLB-4	CGCCAAAATTGCTGCTTTTTGCAGCCGCTGATGCACTCCTCCTTTTTGGAGGTTAAA AACAGGGAAGCGCACAGAGAG
10	2DLB-5	AATTTTTGTTGCTGCTTTTTGCAGCCGCTGATGCACTCCTCCTTTTTGGAGGTTTTTC AATTACCTGAGCAGAGGCGA
12	2DLB-6	ACCAGGCATTGCTGCTTTTTGCAGCCGCTGATGCACTCCTCCTTTTTGGAGGTTTAC CAGAAGGAGCGGATGCGGAAC
14	2DLB-7	AACATACGTTGCTGCTTTTTGCAGCCGCTGATGCACTCCTCCTTTTTGGAGGTTCAA ATGAAAAATCTAACGCTGAGA
16	2DLB-8	CTGTTTGATTGCTGCTTTTTGCAGCCGCTGATGCACTCCTCCTTTTTGGAGGTTGCT CAATCGTCTGAAAATACCTAC
18	2DLB-9	GAAGGGAATTGCTGCTTTTTGCAGCCGCTGATGCACTCCTCCTTTTTGGAGGTTCCG TTAGAATCAGAGCGGGAGCTAA
1	2DLB-10	GGCGGATATTGCTGCTTTTTGCAGCCGCTGATGCACTCCTCCTTTTTGGAGGTTCAA GCCCAATAGGAACCCATGTAC
3	2DLB-11	GACGATTGTTGCTGCTTTTTGCAGCCGCTGATGCACTCCTCCTTTTTGGAGGTTTCCG GTTTATCAGCTTGGGAGCCTT
5	2DLB-12	CCAATGAATTGCTGCTTTTTGCAGCCGCTGATGCACTCCTCCTTTTTGGAGGTTAAA CGAAAGAGGCAAACGAAGGCA
7	2DLB-13	ATGTTAGCTTGCTGCTTTTTGCAGCCGCTGATGCACTCCTCCTTTTTGGAGGTTCCA AATCAACGTAACAACCGGATA
9	2DLB-14	AATAACATTTGCTGCTTTTTGCAGCCGCTGATGCACTCCTCCTTTTTGGAGGTTGGA ATTACGAGGCATAATACATAA
11	2DLB-15	ATTATTCATTGCTGCTTTTTGCAGCCGCTGATGCACTCCTCCTTTTTGGAGGTTTTAA ATCAGCTCATTTCGCATTA
13	2DLB-16	AAAGAACTTGCTGCTTTTTGCAGCCGCTGATGCACTCCTCCTTTTTGGAGGTTAAG CGCCATTCGCCATTGCCGGA
15	2DLB-17	GCCAGCAGTTGCTGCTTTTTGCAGCCGCTGATGCACTCCTCCTTTTTGGAGGTTAG CCGGAAGCATAAAGTTCCACAC
17	2DLB-18	ATTTTGACTTGCTGCTTTTTGCAGCCGCTGATGCACTCCTCCTTTTTGGAGGTTTGG TGTTCCGAAATCCGAAATC

Inner sequence B: AGTGCATCAGCG

FAM-Fuel1: FAM-CCTCCAAAAGGAGG-ATTTCGAGCTC
TAMRA-Fuel2: TAMRA-GCTGCAAAAAGCAGC-CAGAAAATGGC
antiFuel1: GAGCTCGAAT-CCTCCTTTTTGGAGG
antiFuel2: GCCATTTCTG-GCTGCTTTTTGCAGC

References

1. Castro, C.E., *et al.* A primer to scaffolded DNA origami. *Nat Methods* **8**, 221-229 (2011).
2. Woodside, M.T., *et al.* Nanomechanical measurements of the sequence-dependent folding landscapes of single nucleic acid hairpins. *Proc Natl Acad Sci U S A* **103**, 6190-6195 (2006).
3. Alemany, A. & Ritort, F. Determination of the elastic properties of short ssDNA molecules by mechanically folding and unfolding DNA hairpins. *Biopolymers* **101**, 1193-1199 (2014).
4. Simmel, S.S., Nickels, P.C. & Liedl, T. Wireframe and tensegrity DNA nanostructures. *Acc Chem Res* **47**, 1691-1699 (2014).
5. Smith, S.B., Cui, Y. & Bustamante, C. Overstretching B-DNA: The Elastic Response of Individual Double-Stranded and Single-Stranded DNA Molecules. *Science* **271**, 795-799 (1996).
6. Sacca, B., *et al.* Reversible reconfiguration of DNA origami nanochambers monitored by single-molecule FRET. *Angew Chem Int Ed Engl* **54**, 3592-3597 (2015).
7. Peyret, N. Wayne State University (2000).
8. SantaLucia, J. A unified view of polymer, dumbbell, and oligonucleotide DNA nearest-neighbor thermodynamics. *Proc Natl Acad Sci U S A* **95**, 1460-1465 (1998).
9. Zuker, M. Mfold web server for nucleic acid folding and hybridization prediction. *Nucleic Acids Res* **31**, 3406-3415 (2003).
10. Pan, K., *et al.* Lattice-free prediction of three-dimensional structure of programmed DNA assemblies. *Nature Communications* **5**, 5578 (2014).
11. Wei, X., Nangreave, J., Jiang, S., Yan, H. & Liu, Y. Mapping the thermal behavior of DNA origami nanostructures. *J Am Chem Soc* **135**, 6165-6176 (2013).